JACS
JOURNAL OF THE AMERICAN CHEMICAL SOCIETY

Communication

pubs.acs.org/JACS

Facile, Rapid, and Large-Area Periodic Patterning of Semiconductor Substrates with Submicron Inorganic Structures

Thomas J. Kempa,[†] D. Kwabena Bediako,[†] Evan C. Jones,[†] Charles M. Lieber,*[,†,‡] and Daniel G. Nocera*[,†]

[†]Department of Chemistry and Chemical Biology and [‡]School of Engineering and Applied Sciences, Harvard University, Cambridge, Massachusetts 02138, United States

Supporting Information

ABSTRACT: The development of high-throughput and scalable techniques for patterning inorganic structures is useful for the improved function and efficiency of photonic and energy conversion devices. Here we demonstrate a facile and rapid electrochemical method for patterning periodic metallic and nonmetallic submicron structures over large areas. Si substrates have been patterned with arrays of periodically spaced lines, rings, squares, and terraces of main-group and transition-metal oxides. In addition to planar substrates, three-dimensional surfaces and their vertical sidewalls have been patterned. The features are 20(±1) nm high and 360(±15) nm wide, and their period is finely tunable *in situ* from 500 nm to 7 μm. These features exhibit <3% variation in period and are rapidly patterned in <2 min. We demonstrate the versatility of the technique by rapidly patterning an efficient water splitting catalyst, Co phosphate oxide (CoP_i), and show that the integrated materials system performs water splitting with complete Faradaic efficiency. More generally, the ability to pattern submicron structures over large areas in a facile, reliable, and timely manner may be useful for the fabrication of devices for energy, metamaterial, and sensing applications.

Energy-harvesting and conversion devices benefit from semiconducting substrates patterned with inorganic structures. The direct integration of oxidic catalysts for water splitting[1−3] with semiconductor surfaces forms the basis of promising solar-to-fuel conversion devices, such as the artificial leaf.[4] Moreover, semiconductors patterned periodically with metallic and dielectric materials are desirable for enhancing light absorption in solar cells[5] and present opportunities in the context of electrocatalyst-semiconductor devices. Although a repertoire of patterning methods exists,[6−17] development of techniques that are high-throughput, scalable, and simple to implement is useful for the facile fabrication and optimized performance of energy conversion devices,[18] such as the artificial leaf and more generally buried junction devices.[19−21] Here we demonstrate a facile and rapid electrochemical method for patterning periodic metallic, nonmetallic, and catalytic[22] submicron structures over large areas of silicon.

Reactive interface patterning promoted by lithographic electrochemistry (RIPPLE) leads to the formation and propagation of periodically spaced submicron structures over large areas. This new method performs concerted redox etching and patterning of an inorganic material when it is subjected to applied cyclic potentials in the presence of acidic electrolyte. The experimental details of the technique are provided in the Methods section of the Supporting Information. The use of cyclic potentials and a three-electrode configuration affords a high degree of control over the redox processes leading to patterning that is uncommon to electrochemically based patterning methods.[16,17] Application of a linearly ramped potential sweep[23] (0.1−1.2 V; all potentials are referenced to the Ag/AgCl electrode) between a working electrode bearing the material to be patterned and a Pt mesh counter electrode promotes film etching. This etching originates at the site of lines/dots, which were defined through a resist to allow electrolyte access to the material beneath, and then propagates underneath the resist (Figure S1). Figure 1 shows various patterns derived from performing RIPPLE on a Ge film. After applying several cyclic voltammogram (CV) scans to the Ge-coated working electrode and removing the resist, the substrate was examined by scanning electron microscopy (SEM), energy dispersive X-ray spectroscopy (EDS), and atomic force microscopy (AFM). Periodically spaced lines and rings patterned onto the Si substrate (Figure 1a) are observed in SEM images. The parallel lines or concentric rings emanate from the initially defined line or dot, respectively. An SEM survey of several patterns in an array shows that they are composed of well-defined uniform circles (Figure S2). The number of lines or rings formed is given by the empirical expression $N_F = N_{CV} - 1$, where N_F is the number of patterned features and N_{CV} is the number of CV scans. Furthermore, parallel lines patterned at voltage scan rates of 100 and 450 mV s^{-1} exhibit periods of 3.9 μm and 650 nm, respectively (Figure 1b). EDS elemental mapping of the periodic rings and the site at the origin of the pattern, both of which appear as bright contrast in SEM, shows that these features give rise to Ge signal (Figure S2).

The RIPPLE technique is capable of patterning over three-dimensional (3D) surfaces. A Si substrate containing an array of square platforms of 7 μm height was prepared and overlaid with Ge (Figure 1c). Nine lines patterned at a voltage scan rate of 230 mV s^{-1}, originating from the 2 μm wide line positioned atop one of these raised platforms, seamlessly propagate from the top of the platform and then over the edge of the platform (3 lines are positioned on the surface of the vertical edge) and onto the

Received: November 21, 2014
Published: March 5, 2015

DOI: 10.1021/ja5118717
J. Am. Chem. Soc. 2015, 137, 3739−3742

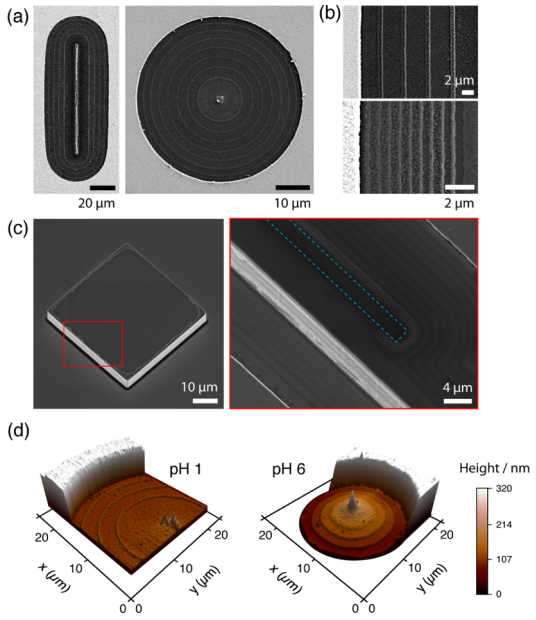

Figure 1. (a) SEM image of patterned periodic features emanating from the site of a defined (left) line and (right) dot. (b) SEM images of periodically spaced and parallel lines patterned from a single line at 100 mV s^{-1} (top) and 450 mV s^{-1} (bottom). (c) SEM image (left) of a square Ge on Si platform raised 7 μm above rest of substrate plane and (right) after patterning of the platform region highlighted with the red box in the left panel. Dashed teal line denotes site where the 2 μm wide line was defined and from which patterns emanate. (d) AFM map of (left) periodically patterned submicron rings and (right) periodic concentric terraces that step down in regular 20 nm increments.

substrate below (Figure 1c). These data highlight a unique feature of RIPPLE to pattern over 3D surfaces and position patterns onto the vertical sidewalls of a raised feature. Unlike most lithographic techniques,[6] the RIPPLE technique is not limited to "line-of-sight" patterning.

An AFM map and line section analysis of the topography of the Ge ring structures show that the periodic, concentric rings are 20(±1) nm high and 360(±15) nm wide and that these dimensions are conserved across the structure (Figures 1d (left) and S3). AFM studies of patterned lines reveal these features have an average height of 20.5(±1.3) nm, which agrees well with measurements for the rings and attests to good uniformity of the features (Figure S3c, Peak A). Root-mean-squared surface roughness (R_{rms}) values calculated from high-resolution AFM maps of the top surface of a Ge line and of the substrate surface between patterned rings reveals R_{rms} = 1.8 and 3.3 nm, respectively (Figure S3d). More complicated 2D to 3D features can be patterned by modifying the electrolyte conditions. An experiment conducted over the same voltage range (0.1−1.2 V) and with a Ge substrate, but at pH 5.9 in the presence of Na_2SO_4, reveals a complex 3D pattern consisting of concentric terraces (R_{rms} = 3.9 nm) which step down in ~20 nm increments from the center region (Figures 1d (right) and S4). This result demonstrates the potential to tune dramatically the morphology of RIPPLE patterns *in situ*.

A detailed analysis of the structure and composition of the patterned features was afforded by high-resolution transmission electron microscopy (HRTEM) and EDS. For imaging purposes, a ~15 nm metal layer was deposited prior to RIPPLE to assist in differentiation of patterned features. Several important features are established by TEM images and EDS maps of an axial cross-section taken at the periphery of a feature containing patterned concentric rings. First, as established by Figure 2a, besides the

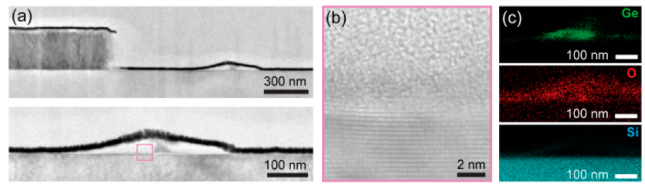

Figure 2. (a) Bright-field TEM images of the axial cross-section of a substrate patterned with concentric rings. (b) High-resolution bright-field TEM image of the interface between the patterned ring and underlying Si substrate marked by the pink box in (a). (c) From top to bottom, EDS elemental maps of Ge, O, and Si for the cross-section of a patterned ring.

patterned ring (bright contrast between substrate and metal layer), there is no material positioned elsewhere on the flat Si substrate. Second, from the HRTEM image of Figure 2b, it appears that the ring has a morphology distinct from that of the underlying ⟨111⟩ Si substrate whose lattice-fringes are visible. EDS elemental Ge and O maps of an area encompassing the ring cross-section (Figure 2c) show significant overlap only in the region of the ring. Together, these data reveal that the patterned submicron structures are composed of an oxide of Ge and that their position on the substrate is highly localized. Finally, the cross-section profile of the rings may be tuned with solvent conditions. Notably, steep and symmetric side-walls are obtained when a surfactant (e.g., sodium dodecyl sulfate) is added to the sulfuric acid electrolyte (Figure S3e).

The production of an oxidic Ge material is consistent with the CV conditions employed for ring formation. The evolution of a single pattern was correlated to SEM images (Figure 3) taken

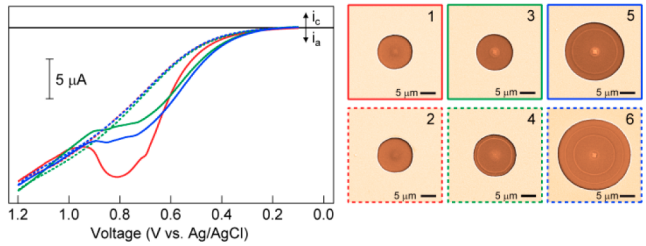

Figure 3. (left) CVs at 100 mV s^{-1} performed in 0.1 M H_2SO_4 and (right) accompanying SEM images of patterned structures. Three CVs, each composed of a forward (solid lines) and reverse (dashed lines) sweep, were performed between 0.1 and 1.2 V (vs Ag/AgCl).

after each forward, 0.1 to 1.2 V, (solid lines, Figure 3) and reverse, 1.2 to 0.1 V, (dashed lines, Figure 3) sweep. At 100 mV s^{-1}, the first forward sweep (solid red line) is characterized by rapid onset of anodic current at ~0.3 V, a broad irreversible peak at 0.81 V, and a linear regime for potentials >0.90 V. These features are preserved in subsequent forward sweeps, and the current associated with the peak at 0.81 V increases monotonically as the pattern increases in size. Reverse sweeps show nearly identical profiles and are absent of any distinguishing features. The CVs are consistent with oxidation of Ge, which is thermodynamically favored to form GeO_2 and soluble H_2GeO_3 (solubility of 43 mM) at pH 1 and at potentials >0 V (0.2 V vs NHE).[24] Indeed, presence of rings comprising Ge and O concurs with EDS data of Figure 2c. Also, an identical patterning experiment conducted at pH 5.9 in the presence of Na_2SO_4

DOI: 10.1021/ja5118717
J. Am. Chem. Soc. 2015, 137, 3739−3742

reveals a CV with quasi-reversible waves between 0.2 and 0.6 V and a pattern consisting of concentric terraces (Figure S4). These results suggest a relation between Ge redox chemistry and germanium oxide solubility, at a given potential and pH, which could be used to tune the profile and composition of the patterns. Furthermore, rings appear during reverse sweeps (Figure 3, images 4 and 6) at a location coincident with the periphery of the etched region formed after the previous forward sweep (Figure 3, images 3 and 5). Finally, when the voltage scan rate was altered in the middle of a patterning process, the period for the first set of rings is consistent with that expected from patterning solely at the first scan rate (Figure S5). From this we conclude that once a Ge feature is patterned, it is not eradicated during ensuing electrochemical processes. Taken together, these data suggest that pattern evolution occurs through oxidation and dissolution of the Ge film in concert with localization of a germanic oxide, which is stable during subsequent electrochemical cycles. Through an apparent interplay of electrochemical and hydrodynamic effects the RIPPLE method allows us to control: (a) the lateral extent of Ge etching via CV and electrolyte conditions, and (b) the formation of features mediated by specific solution conditions, such as pH. The patterns we obtain are akin to those obtained from moving boundary simulations of etching processes.[25] Whereas our results emphasize that pattern formation is electrochemically mediated, capillary flows[26] at the periphery of the unetched parent material may intervene in the formation of periodic features. Work currently underway will allow the proposed mechanism to be more fully defined.

The periodicity of patterned structures produced by the RIPPLE method may be tuned reliably. CVs acquired using voltage scan rates from 30 to 500 mV s^{-1} result in patterned concentric rings with period tunable from 6.9 μm to 537 nm, respectively (Figure 4a). The period for the last ring pair shows a

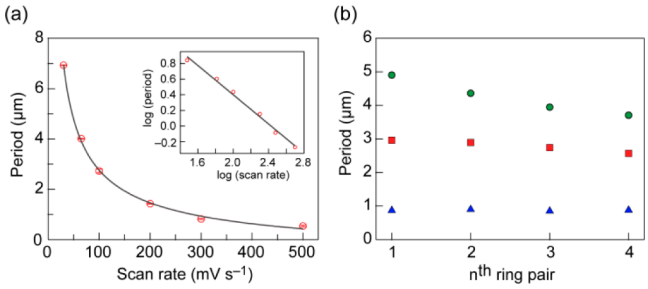

Figure 4. (a) Average period for the last ring pair within randomly sampled patterns as a function of voltage scan rate. Error bars denote % deviation from the mean and the dashed line is a power law fit to the data. Inset: Data presented on a logarithmic plot with linear fit to data. (b) Average period for the first through fourth ring pairs within randomly sampled patterns at 3 different voltage scan rates: 65 (green circle), 100 (red square), and 300 mV s^{-1} (blue triangle).

power law dependence on scan rate (Figure 4 inset) and exhibits <3.0% deviation from the mean among 10 out of 81 patterns randomly sampled over a 0.25 mm^2 area, for each scan rate. For a scan rate of 100 mV s^{-1} there is a 13.3% difference in period between the first and last pair of concentric rings within a pattern (Figure 4b). Notably, for scan rates >300 mV s^{-1}, which yield submicron periods, the deviation in period among all rings within a pattern is <3.1%.

The RIPPLE technique may be used to furnish complex patterns. Hollow Ge squares with micrometer-scale features are formed at the interstices of a square array of closely spaced Ge concentric ring patterns, which were patterned by acquiring 5 CVs at 30 mV s^{-1} (Figure 5a). The combination of rings and

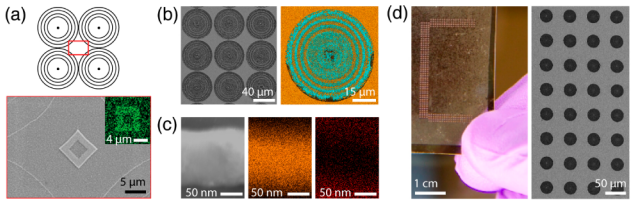

Figure 5. (a) (top) Schematic of a square array of periodic ring patterns. (bottom) SEM image of the region where rings from adjacent patterns overlap with each other. Inset: EDS Ge map of the square. (b) (left) SEM image of an array of rings patterned from a Cu film on Si. (right) Composite Cu (orange) and Si (blue) EDS map of one pattern. (c) (left) High-resolution STEM image of a 60 nm thick axial cross-section of a patterned Cu ring. (middle and right) Cu (orange) and O (red) EDS maps of the same cross-section. (d) (left) Photograph of a Cu-structure patterned over a transparent substrate. (right) SEM image of periodic ring patterns that serve as the "pixels" in design of the patterns.

squares after one round of patterning demonstrates the potential of the RIPPLE technique with regard to creating variegated patterns over large areas of a Si substrate.

The RIPPLE methodology may be extended to patterning metallic materials over large substrate areas. A thin Cu film subjected to 5 CVs between 0.4 and 1.3 V in 0.1 M sulfuric acid leads to formation of concentric rings of Cu over Si (Figure 5b). Copper and oxygen EDS maps of the axial cross-section of a single ring do not overlap, suggesting that the patterned structures are composed of other than an oxide of Cu (Figure 5c). Furthermore, a large shape was patterned from a Cu film on transparent substrate where each "pixel" consisted of a single pattern of concentric Cu rings arranged in a square array (Figure 5d). Together, these data verify that the method may be used to pattern submicron nonmetallic and metallic structures over large areas with control over their shape.

The ability to pattern large substrate areas with metal and oxidic structures suggests the potential for integrating inorganic catalysts with semiconductors for energy conversion applications. We turned our attention to patterning Si with the efficient oxidic cobalt water splitting catalyst, CoP_i.[22] Utilizing the CV conditions as for Cu patterning, a Co film was patterned into concentric ring structures (Figure S6a). Anodization of this patterned Co substrate was performed (Methods and Figure S6b) in accordance with methods that have previously been shown to yield CoP_i.[27] SEM and Co and O EDS maps of the patterned and anodized Co sample reveal well-defined concentric rings composed of the anticipated CoP_i catalyst (Figure 6a). CVs of the CoP_i film exhibit a catalytic wave at 1.0 V (Figure S7) indicative of the water splitting reaction.[22] Furthermore, the significant steady-state catalytic current for potentials $\geq$0.9 V is consistent with that reported for electrodeposited CoP_i films.[22] We conclude from these data that the performance of these patterned systems is comparable to that of bulk films. An oxygen probe experiment carried out over 10 h using this patterned substrate verified the competence of this catalyst toward O_2 generation from water with a Faradaic efficiency of >99% (Figure 6b). Electrolysis performed for over 20 h also verified the well-established stability of the catalyst (Figure S8).

The RIPPLE technique directly patterns arrays of periodically spaced submicron scale structures of inorganic materials onto

DOI: 10.1021/ja5118717
J. Am. Chem. Soc. 2015, 137, 3739−3742

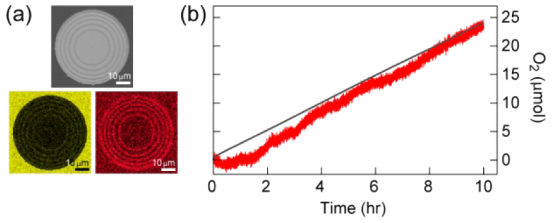

Figure 6. (a) RIPPLE-patterned oxidic cobalt phosphate (CoP_i) water splitting catalyst on a platinum/silicon substrate: (top) SEM image of CoP_i catalyst patterned into concentric rings; and (bottom left and right) Co (yellow) and O (red) EDS maps of a single CoP_i catalyst pattern. (b) O_2 evolved by patterned CoP_i catalyst as measured by a fluorescent probe (red) and O_2 calculated from charge passed assuming a Faradaic efficiency of 100% (black).

planar and 3D semiconducting substrates. The process is reliable, applicable to wafer-scale and even larger substrates, and fast with the CV cycling directly associated with patterning. Considering all steps intrinsic to preparation and patterning, the process takes <30 min and can yield multiple substrates patterned in parallel. Furthermore, unlike most forms of conventional lithography,[6] RIPPLE is not limited to "line-of-sight" patterning and has been used to pattern 3D surfaces and their vertical sidewalls. This unique feature may allow for positioning of catalysts over textured substrates, such as those with high aspect ratio features. Optimized integration of catalysts with semiconductors may enable improved solar-to-fuel conversion devices, which benefit from photon management and reduced optical losses owing to absorption by the catalyst material. Given the fidelity of and *in situ* control over RIPPLE patterned structures and their period, future work will also investigate their role in photonic and plasmonic applications.[28−31] Capitalizing on such applications requires fabricating high-quality optical elements characterized by low surface roughness, sharp pattern profiles, and a small dispersion in submicron periods. It may be beneficial from the standpoint of materials efficiency to modify RIPPLE so that it functions in a strictly additive sense with periodic deposition occurring from solution-phase precursors supplied via microfluidic arrays. These and other imperatives will motivate future efforts, including exploration of the fundamental resolution, material limits, and mechanism of this patterning. The high-throughput, facile, and large area patterning of submicron inorganic structures by RIPPLE could enable new and emerging opportunities in energy conversion and storage.

■ ASSOCIATED CONTENT

Supporting Information

Detailed description of materials and methods and figures. This material is available free of charge via the Internet at http://pubs.acs.org.

■ AUTHOR INFORMATION

Corresponding Authors

*dnocera@fas.harvard.edu
*cml@cmliris.harvard.edu

Notes

The authors declare no competing financial interest.

■ ACKNOWLEDGMENTS

D.G.N. acknowledges support by NSF CCI Center CHE-1305124. C.M.L. acknowledges support from a Department of Defense NSSEFF Award (N00244-09-1-0078). We thank David Bell, Adam Graham, and Nicholas Antoniou for assistance with FIB. We thank J. Garcia for his contributions to RIPPLE.

■ REFERENCES

(1) Man, I. C.; Su, H.-Y; Calle-Vallejo, F.; Hansen, H. A.; Martinez, J. I.; Inoglu, N. G.; Kitchin, J.; Jaramillo, T. F.; Norskov, J. K.; Rossmeisl, J. *ChemCatChem* **2011**, *3*, 1159.
(2) Surendranath, Y.; Nocera, D. G. *Prog. Inorg. Chem.* **2011**, *57*, 505.
(3) Suntivich, J.; May, K. J.; Gasteiger, H. A.; Goodenough, J. B.; Shao-Horn, Y. *Science* **2011**, *334*, 1383.
(4) Nocera, D. G. *Acc. Chem. Res.* **2012**, *45*, 767.
(5) Atwater, H. A.; Polman, A. *Nat. Mater.* **2010**, *9*, 205.
(6) Madou, M. J. Fundamentals of Microfabrication and Nanotechnology. *Manufacturing Techniques for Microfabrication and Nanotechnology*, 3rd ed.; CRC Press: Boca Raton, FL, 2011; Vol. *II*.
(7) Lehn, J.-M. *Angew. Chem., Int. Ed. Engl.* **1990**, *29*, 1304.
(8) Xia, Y.; Gates, B.; Yin, Y.; Lu, Y. *Adv. Mater.* **2000**, *12*, 693.
(9) Jeong, S.; Hu, L.; Lee, H. R.; Garnett, E.; Choi, J. W.; Cui, Y. *Nano Lett.* **2010**, *10*, 2989.
(10) Rothemund, P. W. K. *Nature* **2006**, *440*, 297.
(11) Nykypanchuk, D.; Maye, M. M.; van der Lelie, D.; Gang, O. *Nature* **2008**, *451*, 549.
(12) Melosh, N. A.; Boukai, A.; Diana, F.; Gerardot, B.; Badolato, A.; Petroff, P. M.; Heath, J. R. *Science* **2003**, *300*, 112.
(13) Piner, R. D.; Zhu, J.; Xu, F.; Hong, S.; Mirkin, C. A. *Science* **1999**, *283*, 661.
(14) Xia, Y.; Whitesides, G. M. *Annu. Rev. Mater. Sci.* **1998**, *28*, 153.
(15) Meitl, M. A.; Zhu, Z. T.; Kumar, V.; Lee, K. J.; Feng, X.; Huang, Y. Y.; Adesida, I.; Nuzzo, R. G.; Rogers, J. A. *Nat. Mater.* **2006**, *5*, 33.
(16) Simeone, F. C.; Albonetti, C.; Cavallini, M. *J. Phys. Chem. C* **2009**, *113*, 18987.
(17) Li, W.; Virtanen, J. A.; Penner, R. M. *Appl. Phys. Lett.* **1992**, *60*, 1181.
(18) James, B. D.; Baum, G. N.; Perez, J.; Baum, K. N. *Technoeconomic Analysis of Photoelectrochemical (PEC) Hydrogen Production*; Directed Technologies: Arlington, VA, 2009.
(19) Hanna, M. C.; Nozik, A. J. *J. Appl. Phys.* **2006**, *100*, 074510/1.
(20) Cox, C. R.; Winkler, M. T.; Pijpers, J. H.; Buonassisi, T.; Nocera, D. G. *Energy Environ. Sci.* **2013**, *6*, 532.
(21) Surendranath, Y.; Bediako, D. K.; Nocera, D. G. *Proc. Natl. Acad. Sci. U.S.A.* **2012**, *109*, 15617.
(22) Surendranath, Y.; Kanan, M. W.; Nocera, D. G. *J. Am. Chem. Soc.* **2010**, *132*, 16501.
(23) Savéant, J.-M. *Elements of Molecular and Biomolecular Electrochemistry*; Wiley-Interscience: Hoboken, NJ, 2006.
(24) Pourbaix, M. *Atlas of Electrochemical Equilibria in Aqueous Solutions*; Pergamon Press: Oxford, 1966.
(25) West, A. C.; Madore, C.; Matlosz, M.; Landolt, D. *J. Electrochem. Soc.* **1992**, *139*, 499.
(26) Deegan, R. D.; Bakajin, O.; Dupont, T. F.; Huber, G.; Nagel, S. R.; Witten, T. A. *Nature* **1997**, *389*, 827.
(27) Young, E. R.; Nocera, D. G.; Bulovic, V. *Energy Environ. Sci.* **2010**, *3*, 1726.
(28) Delacour, C.; Blaize, S.; Grosse, P.; Fedeli, J. M.; Bruyant, A.; Salas-Montiel, R.; Lerondel, G.; Chelnokov, A. *Nano Lett.* **2010**, *10*, 2922.
(29) Kim, S.-K.; Ee, H.-S.; Choi, W.; Kwon, S.-H.; Kang, J.-H.; Kim, Y.-H.; Kwon, H.; Park, H.-G. *Appl. Phys. Lett.* **2011**, *98*, 011109.
(30) Jun, Y. C.; Huang, K. C. Y.; Brongersma, M. L. *Nat. Commun.* **2011**, *2*, 283:1.
(31) Zhou, W.; Dridi, M.; Suh, J. Y.; Kim, C. H.; Co, D. T.; Wasielewski, M. R.; Schatz, G. C.; Odom, T. W. *Nat. Nanotechnol.* **2013**, *8*, 506.

DOI: 10.1021/ja5118717
J. Am. Chem. Soc. 2015, 137, 3739−3742